Soliton formation in an exciton-polariton condensate at a bound state in the continuum

I. Septembre [1,*] I. Foudjo,[1] V. Develay [2] T. Guillet,[2] S. Bouchoule,[3] J. Zúñiga-Pérez [4,5]
D. D. Solnyshkov [1,6] and G. Malpuech[1]

[1]*Université Clermont Auvergne, Clermont Auvergne INP, CNRS, Institut Pascal, F-63000 Clermont-Ferrand, France*
[2]*Laboratoire Charles Coulomb, Université de Montpellier, CNRS, 34095 Montpellier, France*
[3]*Centre de Nanosciences et de Nanotechnologies, CNRS, Université Paris-Saclay, 91120 Palaiseau, France*
[4]*UCA, CRHEA-CNRS, Rue Bernard Gregory, 06560 Valbonne, France*
[5]*MajuLab, International Research Laboratory IRL 3654, CNRS, Université Côte d'Azur, Sorbonne Université,
National University of Singapore, Nanyang Technological University, Singapore 117543, Singapore*
[6]*Institut Universitaire de France (IUF), 75231 Paris, France*

Bound states in the continuum (BICs) are of special interest in photonics due to their theoretically infinite radiative lifetime. In this work, we take a specific example (a structure composed of GaN and a TiO_2 photonic crystal slab), showcasing how the interactions affect BICs. The photonic BIC hosted by the photonic crystal slab couples with the excitons of GaN to form a polaritonic BIC with a negative mass. This allows condensation to be reached with a low threshold in a structure suitable for electrical injection, paving the way for room-temperature polariton microdevices. We study in detail how the repulsive interaction between exciton-polaritons affects the condensate distribution in reciprocal space and, consequently, the condensate's overlap with the BIC resonance and, therefore, the condensate lifetime. We study an intrinsic contribution related to the formation of a bright soliton and the extrinsic contribution related to the interaction with an excitonic reservoir induced by spatially focused nonresonant pumping. We then study the peculiar dynamics of the condensation process in a BIC state for interacting particles using Boltzmann equations and hybrid Boltzmann–Gross-Pitaevskii equations. We find optimal conditions allowing one to benefit from the long lifetime of the BIC for polariton condensation in a real structure.

I. INTRODUCTION

A large part of physics is built upon the conservation of quantities, such as energy or momentum, related to symmetries [1]. This is the case of the Hamiltonian description of classical mechanics and then of quantum mechanics. However, the irreversible decay of a particle or a mode because of its coupling to a continuum is ubiquitous and, therefore, essential to describe various phenomena. Techniques have been developed, for example in quantum optics, which separate the reversible Hamiltonian dynamics and the dissipative dynamics related to the irreversible decay toward a continuum [2]. A somewhat simpler description of multimode nonconservative systems came with the development of non-Hermitian theories, where modes have complex energies with imaginary parts describing their decay [3]. The coupling between two such modes hybridizes them but also redistributes [4] their imaginary parts $\Gamma_{1,2}$. In the case of a Hermitian coupling, the maximal redistribution occurs at exceptional points (EPs), where the mode decay becomes the mean value of that of the uncoupled modes $(\Gamma_1 + \Gamma_2)/2$. It can be zero only in systems with equal gain and loss (*PT*-symmetric) for the original modes. The study of non-Hermitian systems and in particular of EPs became extremely popular in the last decade

[5], partly because of the possibility offered to control the decay of the modes. This is essential for many applications including lasing [6], and can even lead to fundamentally new concepts, such as the non-Hermitian skin effect [7,8].

Extra opportunities in this quest of controlling lifetimes came from the so-called dissipative coupling introduced in the 1980s [9]. The idea is that two modes are coupled to the same continuum, and because of this coupling, a transfer of particles from one mode to another can take place with a rate computed as $i\sqrt{\Gamma_1\Gamma_2}$ [10]. This non-Hermitian term offers a new resonance condition, where one eigenmode of the coupled system becomes entirely nondecaying. This type of mode is called a bound state in the continuum (BIC) [11]. It was described long ago in the context of quantum mechanics [12], but BICs in photonic systems appear very appealing and commonly present [13]. BICs in photonic crystal slabs or metasurfaces are modes that lie above the light cone but are not coupled to the far field. One should note that other decay mechanisms, such as disorder-induced elastic scattering toward other modes, are not suppressed for BICs, which means that, in reality, their lifetime is finite. In the 2000s, when photonic crystal slabs became widely studied, a very important goal was to improve the lifetime of the modes to realize lasers, but the BIC concept had not yet been established. Nevertheless, experimental and theoretical works found that modes with a long lifetime could be realized near the Γ point of photonic crystal dispersion [14,15]. Here, the BICs form

---

*Corresponding author: ismael.septembre@uca.fr

when two modes of the same polarization and parity couple through the continuum.

Recently, BICs have been implemented in strongly coupled exciton-photon systems where exciton-polaritons (polaritons) form with transition metal dichalcogenides (TMDs) [16–18] and GaAs active regions [19,20]. As expected, nonresonantly pumped polaritons were found to accumulate in the state with the longest lifetime, namely the BIC state, forming a Bose-Einstein condensate (BEC) [21,22]. A principal advantage of a polariton condensate versus a photon laser is that the transparency condition required for lasing is not necessary for polariton lasing [23,24]. The only lasing condition for polaritons (which is also present for photon lasers) is that scattering toward a state overcomes its losses, which are expected to be essentially radiative losses for polaritons and that vanish for BICs. Another key difference between polaritons and bare photons is that polaritons are interacting particles. They interact with themselves and with reservoir excitons created by an external pumping. Depending on the sign of the effective mass, these interactions, which are typically repulsive, can either tend to delocalize particles [25] in real space or localize them, forming bright solitons [26,27] or simply reservoir-induced localized states [28]. In systems with both positive and negative mass states, the localization near the exciton reservoir induced by the pump on negative mass states tends to favor condensation in these states [26,28,29]. An important consequence of the formation of either a soliton-like BEC or of a BEC bound to a spatially localized exciton reservoir is that it broadens the condensate distribution in k space. Finally, a BIC-based polariton BEC has been demonstrated in GaAs-based structures at low temperature [21,22]. The potential use of polariton-based devices requires room-temperature operation, which is typically implemented either using large-band-gap semiconductors (ZnO [30–32], GaN [33–35]), organic materials [36,37], or perovskites [38–40]. In that perspective, GaN-based devices remain the best potential choice since this material offers the best stability as an inorganic semiconductor, and also the possibility to fabricate electrically injected devices. In recent works [21,41,42], the specific features of polariton BICs were investigated experimentally and theoretically. However, the effect of the interactions on the shape of the condensate and the resulting losses has not been investigated.

In this work, we propose to deepen the understanding of the phenomenology related to interacting photonic (e.g., polaritonic) condensates in BICs. Indeed, we go further than previous models and take into account the extension of the interacting state (soliton) in reciprocal space, and not only the high lifetime of the BIC. We also use coupled Boltzmann–Gross-Pitaevskii equations to find the stationary states and estimate the condensation threshold in several experimentally accessible configurations.

The paper is organized as follows. We first propose a design of a realistic BIC-based polariton laser in a GaN/TiO$_2$ polaritonic crystal slab, using finite-element methods to solve Maxwell's equations. We then use this structure as an example to study analytically and numerically polariton-specific features, particularly the role played by interactions (which is remarkably interesting for materials such as wide-band-gap semiconductors and TMDs). In the conservative limit, we

determine the shape of the polariton BEC with and without the reservoir potential. This allows us to analytically compute the average BEC particle lifetime in both cases. We then use the computed lifetimes to model quantitatively the polariton condensation using Boltzmann equations. We find that the advantage of having a BIC is strongly reduced, if not canceled, when the interaction with a reservoir reduces too strongly the condensate extension in real space (so it broadens in k space), explaining recent experimental results [41]. We find that even without any confinement from the reservoir, the formation of a soliton provides anyway an intrinsic limitation to the lifetime enhancement provided by the BIC, although the threshold can still be reduced by more than one order of magnitude. At large pumping density, the formation of a soliton provides saturation of the condensate density growth rate versus pumping, which scales as $P^{1/3}$ instead of being linear. Finally, we model the polariton condensation process, solving numerically hybrid Boltzmann–Gross-Pitaevskii equations [43], which allows us to take into account self-consistently the energy relaxation and the interparticle interactions.

II. STRUCTURE DESIGN

In this section, we describe a possible structure that can be used to obtain a BIC at room temperature. The purpose is to give a concrete example of how a photonic BIC can arise in a structure with exciton-polaritons using a promising platform for reaching electrical injection at room temperature (GaN). However, the results obtained in the sections following the present one are not specific to this structure but can be applied to any interacting photonic BIC, up to the extent that the parameters (for instance, the strength of the interactions) may change considerably.

The structure we consider is sketched in Fig. 1(a). It is composed of a TiO$_2$ slab deposited on top of a GaN waveguide. The GaN slab is isolated from the bulk GaN substrate by a cladding layer, which we choose to be Al$_x$Ga$_{1-x}$N, with $x \approx 0.2$, as often done in experiments [35]. The TiO$_2$ layer is patterned with a 1D step pattern, forming a photonic crystal slab. Its lattice constant is denoted a_0. The width of the steps is a_1, while the space between them is a_2, with $a_1 + a_2 = a_0$.

We simulate the structure in COMSOL and find the dispersion relation of the photonic modes $E_p(k)$, together with their radiative losses $\Gamma_r(k)$. The structural parameters we use are $a_0 = 135$ nm, $a_1 = 80$ nm, $a_2 = 55$ nm, $h_0 = 50$ nm, and $h_{GaN} = 100$ nm. The dispersion relation is plotted in Fig. 1(b) (dashed lines). We see that there are two photonic branches, both behaving quadratically for low wave vectors. We call the negative-mass photonic branch the "BIC" branch because it contains the BIC (at $k = 0$), while the branch at higher energy is called the "lossy" branch because the states are lossy at all wave vectors. A dashed arrow indicates the photonic BIC (state) at $k = 0$. We can approximate the photonic dispersion relation with a quadratic dispersion of the form

$$E_p^{\text{BIC/lossy}}(k) = E_{0,p}^{\text{BIC/lossy}} + \frac{\hbar^2 k^2}{2m_p^{\text{BIC/lossy}}}, \quad (1)$$

where $\hbar$ is the reduced Planck's constant and m_p the photonic effective mass. $E_{0,p}$ is the energy of the branches at $k = 0$. The
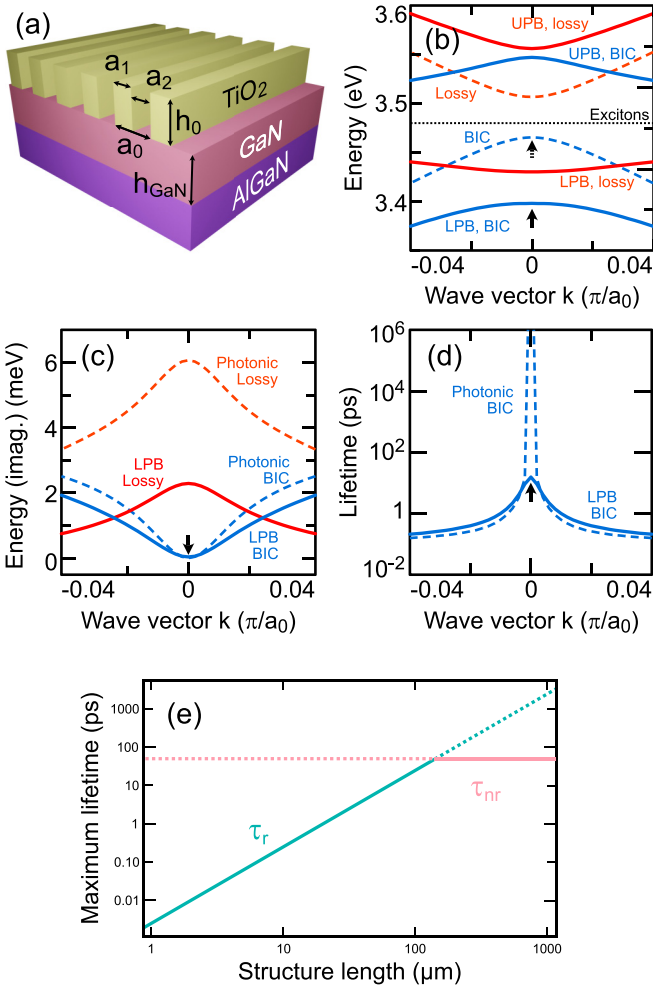
FIG. 1. (a) Sketch of the photonic crystal slab structure studied. A two-layer waveguide (TiO₂ in yellow and GaN in pink) is separated from the substrate by a cladding layer (AlGaN in purple). The TiO₂ layer is etched with a steplike profile (step width a_1). (b) Photonic dispersion relation (dashed lines) for the branch containing a BIC (BIC branch, in blue) and the branch containing no BIC (lossy branch, in red). The corresponding polaritonic dispersion relations are plotted in solid lines (red/blue for the polariton dispersion relation calculated from the photonic lossy/BIC branch, respectively). There are two polariton branches (upper/lower polariton branch) for each photonic branch. The exciton effective energy is indicated as a dotted line. We extract m from the BIC LPB. (c) Imaginary part of the energy of the photonic branches (dashed lines) and lower polaritonic branches (solid lines) versus wave vector. The red/blue curve corresponds to the lossy/BIC branch. We extract Λ from the BIC LPB. (d) Photonic/polaritonic (dashed/solid line) lifetime (log scale) against wave vector. (e) Maximum lifetime achievable depending on the structure length L. The blue/pink lines indicate the radiative/nonradiative lifetimes. In (b)–(d), the polaritonic/photonic BIC at $k = 0$ is indicated with a solid/dashed black arrow.

lossy branch has a positive mass, while the BIC branch has a negative one in our case. This can be inverted by tuning the parameters, particularly the filling factor a_1/a_0.

In Fig. 1(c), we show the radiative losses (imaginary part of the energy, $\hbar\Gamma$) of the photonic modes. We can see that while the radiative losses of the BIC branch are zero for $k = 0$, the

losses of the lossy branch are always nonzero. Similarly to the real part of the energy, the imaginary part can be approximated by a square dependence on the wave vector:

$$\Gamma_r^{\text{BIC/lossy}}(k) = \Gamma_{r0}^{\text{BIC/lossy}} + \gamma_r^{\text{BIC/lossy}}k^2, \qquad (2)$$

where Γ_{r0} are the radiative losses at $k = 0$. For the BIC branch, this term is zero because the losses vanish at the BIC at $k = 0$:

$$\Gamma_r^{\text{BIC}}(k) = \gamma_r k^2. \qquad (3)$$

In our simulations, we neglect the imaginary part of the permittivity of the materials. This is possible because, for the specific structure we consider, the imaginary part of the permittivity is 3–4 orders of magnitude lower than its real part at the energy of the BIC. Most of this absorption corresponds to the creation of excitons, which is properly accounted for by the strong-coupling Hamiltonian below. This is what allows the observation of high quality factors for polaritonic modes in GaN [44].

We can calculate the lifetime of the modes from the radiative losses as

$$\tau_r(k) = \frac{1}{2\Gamma_r(k)}, \qquad (4)$$

and we see that the radiative lifetime of the BIC is theoretically infinite, as can be seen in Fig. 1(d). However, several limitations prevent real BICs from having an infinite lifetime. The first limitation results from the finite size of the structure. Indeed, the size of the full structure L limits the minimal wave vector that can be achieved $k_{\min} \approx \frac{2\pi}{L}$. The radiative lifetime of the BIC branch is infinite only at $k = 0$, so since this value is not achievable, the radiative lifetime of an ideal photonic BIC is limited to

$$\tau_{\max}^{\text{BIC}} = \frac{L^2}{8\pi^2\gamma_r}. \qquad (5)$$

This is represented in Fig. 1(e) as a green line: the larger the structure, the longer the radiative lifetime, but a real (finite) structure will never exhibit an infinite lifetime. Moreover, nonradiative losses can also play an important role, as we explore in the following.

We designed the structure so that the energies of interest are close to the excitonic resonance of GaN. The photonic modes will thus couple to the excitonic modes and form exciton-polaritons, which are part-light, part-matter quasiparticles. To find the polaritonic dispersion relation out of the photonic dispersion relation containing the lossy branch and the BIC branch, we consider the strong coupling between excitons and photons through the effective strong-coupling Hamiltonian:

$$M_{\text{SC}} = \begin{pmatrix} E_X(k) & \rho\hbar\Omega_R/2 & 0 & 0 \\ \rho\hbar\Omega_R/2 & E_p^{\text{lossy}}(k) & 0 & 0 \\ 0 & 0 & E_X(k) & \rho'\hbar\Omega_R/2 \\ 0 & 0 & \rho'\hbar\Omega_R/2 & E_p^{\text{BIC}}(k) \end{pmatrix}, \qquad (6)$$

where $E_X(k) \approx E_X = 3480$ meV at 5 K and 3520 meV at room temperature [45,46] is the effective excitonic resonance of GaN, which groups both A and B exciton contributions.

The two different photonic modes have distinct spatial distributions and are coupled to distinct spatial distributions of excitons, which explains the structure of the Hamiltonian. $E_p(k)$ are the photonic dispersions found in COMSOL, and we take the Rabi splitting $\hbar\Omega_R = 100$ meV for GaN [45]. ρ and ρ' are the fractions of the lossy/BIC modes, respectively, that are located in the GaN layer. Indeed, since the waveguide is composed not only of GaN but also of a TiO$_2$ photonic crystal slab, which does not contain excitons, we take it into account in the overlap integral between the photon and excitons wave functions, which sets the Rabi splitting value, as we did previously [47]. In our design, the value of ρ is typically around 60%, while the value of ρ' is close to 75%. The polaritonic dispersion arising from the strong coupling between excitons and photons is determined by finding the eigenvalues of the matrix M_{SC}. The polaritonic dispersions read

$$E_\pm(k) = \frac{E_X + E_p(k)}{2} \pm \frac{1}{2}\sqrt{(\rho\hbar\Omega_R)^2 + [E_X - E_p(k)]^2}, \quad (7)$$

where the $+$ sign corresponds to the upper polariton branches (UPBs) with energies above the exciton resonance, and the sign corresponds to the lower polariton branches (LPBs) whose energies lie below the exciton resonance.

We plot the resulting polaritonic dispersion in solid lines in Fig. 1(b). The exciton energy is represented as a dotted black line, which is horizontal because the mass of the excitons is orders of magnitude larger than the effective mass of photons. One obtains four polaritonic branches from the two excitonic and two photonic modes. The UPB and LPB corresponding to the BIC (blue) and lossy (red) branches are shown in the figure. The main branch of interest for us is the BIC LPB, represented as a solid blue line with an energy below the exciton energy. The BIC is located at $k = 0$ and indicated by a black arrow. We see that at low wave vectors, the dispersion relation of this branch can be approximated by a quadratic dependence on the wave vector:

$$E(k) \approx E_0^{BIC} + \frac{\hbar^2 k^2}{2m}, \quad (8)$$

where $m = -(1.5 \pm 0.1) \times 10^{-6}m_0$ is the fitted polariton mass, m_0 being the free electron mass. This effective mass is negative. E_0^{BIC} is the energy of the BIC LPB branch at $k = 0$.

In the strong-coupling regime, the imaginary part of the polariton energy Γ can be expressed as [24]

$$\Gamma = C_X(k)\Gamma_X + [1 - C_X(k)]\Gamma_p(k), \quad (9)$$

where $\Gamma_{p,X}$ are the losses of the photonic/excitonic modes, respectively, and C_X is the exciton fraction. This fraction can be modulated by engineering the dispersion relation; more precisely, it depends on the detuning between the exciton energy and the photonic energy at $k = 0$. Thus, by engineering the structure (period, etc.), one can increase the excitonic part of the polaritonic modes and consequently increase the interactions, which have been experimentally measured in GaN just recently [48].

The lifetime of the polaritons, as that of the photonic modes, can be fitted by a quadratic dependence on the wave vector for small k. The approximate expression is given by

$$\hbar\Gamma_{pol}(k) \approx \hbar\Gamma_0 + \Lambda\frac{\hbar^2 k^2}{2m}, \quad (10)$$

where Γ_0 are the constant losses and $\Lambda = -0.27 \pm 0.03$ is obtained from a fitting. Λ is negative here because m is negative while the losses increase with the wave vector for the BIC branch.

Ultimately, the nonradiative lifetime introduced by the excitons will limit the lifetime of a polaritonic BIC. According to Ref. [49], the order of magnitude of the nonradiative excitonic lifetime is 50 ps at room temperature in GaN. This means that the longest lifetime possible for a polaritonic BIC in this structure is limited, even in an infinite structure. Figure 1(e) shows that the lifetime of the BIC is limited by the size of the structure when the structure is small but finally, for large structures, the nonradiative lifetime will limit the polaritonic lifetime. Still, depending on the parameters, very high lifetimes can be observed in realistically large structures. For a structure of 100 µm length, the lifetime achieved thanks to the BIC is of the order of 20 ps, corresponding to a quality factor of $Q \approx 20\,000$. For a room-temperature operation, this is a high value compared to the literature with guided modes [50] (and here, the mode is above the light cone). In cavities, condensation has been observed already for quality factors close to 1000 [34,51,52], which is much lower than the value we found. Even if we consider a 5% uncertainty on the geometrical parameters in the fabricated structure, we estimate from numerical simulations that the quality factor in our structure can be of the order of 5000, so it would still allow polariton condensation. For larger structures, the lifetime is ultimately limited by the nonradiative lifetime, not by the structure's size.

III. INFLUENCE OF THE INTERACTIONS ON THE LIFETIME

In this section and the following, we quantify the influence of the interactions on the lifetime of a BEC originating from a BIC. We will take the structure simulated in the previous section as an example, but the formalism could be applied to any photonic structure containing interacting particles. In particular, we want to stress that it is particularly adequate to consider these effects when studying photonic BICs coupled to dipolar excitons provided by 2D materials, such as transition metal dichalcogenides (TMDs), for which the interactions are very strong [53–55].

In this section, we use the k-dependent losses of the BIC to compute the losses of the states hosted by the structure. Indeed, as shown in the previous section, the decay rates (and lifetimes) of modes around the BIC are strongly k dependent (this feature is universal and not specific to the particular structure studied here). An ideal noninteracting homogeneous condensate would occupy a single state $k = 0$ and benefit from the corresponding extremely long lifetime. However, different mechanisms can lead to a localization of the condensate in real space and thus to a broadening in k space, leading to an increase in the overall condensate decay rate (decrease of the

lifetime). This contribution can be computed as

$$\langle \Gamma_{\text{pol},r} \rangle = \frac{1}{N} \int \Gamma_{\text{pol},r}(k) |\psi(k)|^2 dk, \tag{11}$$

where $\psi(k)$ is the k component of the condensate wave function normalized to the number N of condensed particles and $\hbar \Gamma_{\text{pol},r}(k) = \Lambda \hbar^2 k^2 / 2m$ is the wave-vector-dependent part of the polariton decay rate (10).

There are two localization mechanisms in real space for negative-mass particles with repulsive interactions. The first one is an intrinsic mechanism related to the formation of a bright soliton, whose width is related to N. The second mechanism takes place if the pump is nonuniform (localized) in real space. The generated excitonic reservoir repulsively interacts with the condensate, playing the role of an attractive potential. Generally, both mechanisms are present [26]. We first treat this problem analytically, using the conservative Gross-Pitaevskii (GP) equation,

$$i\hbar \frac{\partial \psi}{\partial t} = -\frac{\hbar^2}{2m} \frac{\partial^2 \psi}{\partial x^2} + \alpha |\psi|^2 \psi + U(x) \psi, \tag{12}$$

where α is the polariton-polariton interaction constant and $U(x)$ an external potential induced by the exciton reservoir. This equation describes contact interactions, and so our results cannot be directly applied to dipolar exciton-polariton systems.

So far, the losses have been neglected. We start with the intrinsic mechanism of bright soliton formation [without any external potential $U(x) = 0$]. The bright soliton solution of the GP equation without external potential reads

$$\psi_s = \frac{\psi_s^{(0)}}{\cosh(x/\sqrt{2}\xi)}, \tag{13}$$

where ξ is the healing length defined as

$$\xi = \frac{\hbar}{\sqrt{2|m\alpha|}\psi_s^{(0)}} \tag{14}$$

and $\psi_s^{(0)}$ is the value of the wave function at $x = 0$, defined as

$$\psi_s^{(0)} = \frac{\sqrt{|m\alpha|N}}{2\hbar}, \tag{15}$$

which ensures the normalization of the wave function to N. Finally, the healing length can be rewritten explicitly as a function of N as

$$\xi = \frac{\sqrt{2}\hbar^2}{|m\alpha|N}. \tag{16}$$

This shape allows us to compute analytically the decay rate in the presence of a BIC using formula (11) as

$$\langle \hbar \Gamma_r \rangle = \Lambda \frac{\alpha^2 m}{12\pi^2 \hbar^2} N^2. \tag{17}$$

This nonlinear loss rate will saturate the growth of N after the condensation threshold. Qualitatively, the accumulation of particles in the soliton renders it larger in k space, which increases the decay rate, which then limits the growth of N.

We now consider the localization by an external potential induced by the finite size of a Gaussian reservoir created by a nonresonant pumping:

$$U(x) = U_0 e^{-\frac{x^2}{2\sigma^2}}, \tag{18}$$

where U_0 is the height of the potential "trap" formed by the pump and σ is its width in real space. The full width at half maximum (FWHM) of the pump is $2\sqrt{2\ln(2)}\sigma$. We approximate the potential by a parabolic profile found from the Gaussian profile by a series expansion:

$$U \approx U_0 \left(1 - \frac{x^2}{\sigma^2} \right). \tag{19}$$

The solutions to the Schrödinger equation for negative-mass particles in this harmonic potential correspond to the solutions for positive-mass particles but with a potential $-U$. The solutions are the well-known states of the harmonic oscillator, which are the products of Hermite polynomials and of a Gaussian function. This harmonic oscillator description is valid only for particle energies within the gap between the BIC and lossy branches. This limits the number of modes confined by the potential and, in practice, we will only consider the two first modes $\tilde{\psi}_{0,1}$ defined as

$$\tilde{\psi}_0 = \frac{1}{\sqrt{w\sqrt{\pi}}} e^{-\frac{x^2}{2w^2}}, \quad \tilde{\psi}_1 = \sqrt{2}\frac{x}{w}\tilde{\psi}_0, \tag{20}$$

where w is the width of the Gaussian wave function. The state 1 is expected to host a condensate when the energy of the state 0 becomes larger than the gap and is therefore not confined anymore [26,28,41,42].

Because of the presence of both the interactions and the potential, the Gross-Pitaevskii equation is not exactly solvable. We use the variational approach to find the solution analytically, using the width w of the Gaussian wave function as a variational parameter. We start with a trial wave function of a Gaussian shape, given by $\psi_0 = \sqrt{N}\tilde{\psi}_0$, where N is the number of particles (note that $\int |\psi_0|^2 dx = N$ while $\int |\tilde{\psi}_0|^2 dx = 1$). We then find the width w that minimizes the total energy of the system E_{tot}, which is the sum of the kinetic, potential, and interaction energy:

$$E_{\text{tot}} = E_{\text{kin}} + E_{\text{pot}} + E_{\text{int}}. \tag{21}$$

The minimization condition allows us to write an equation for w that we solve:

$$\frac{\partial E_{\text{tot}}}{\partial w} = 0. \tag{22}$$

The different energy terms are calculated from the trial wave function as follows [25]:

$$E_{\text{kin}} = \int -\psi_0^* \frac{\hbar^2}{2m} \frac{\partial^2 \psi_0}{\partial x^2} dx, \tag{23}$$

$$E_{\text{pot}} = \int |\psi_0|^2 U dx, \tag{24}$$

$$E_{\text{int}} = \int \frac{\alpha}{2} |\psi_0|^4 dx. \tag{25}$$

In the end, we find the total energy, written here per particle:

$$E_{\text{tot}}/N = \frac{\hbar^2}{4mw^2} + \frac{w^2 U_0}{\sigma^2} + \frac{\alpha N}{2\sqrt{2\pi}w}. \tag{26}$$

In the absence of interactions ($\alpha = 0$), the energy is minimized for a width [56,57]

$$w_{|\alpha=0} \equiv w_0 = \sqrt{\frac{\hbar\sigma}{\sqrt{|m|U_0}}}. \quad (27)$$

The trial function is an exact solution in this case. The decay rate can be found analytically. It reads

$$\langle \Gamma_{r,0} \rangle = \frac{\pi \Lambda \hbar}{2mw^2}. \quad (28)$$

A similar analysis can be made for state 1, and the decay rate reads

$$\langle \Gamma_{r,1} \rangle = 3 \langle \Gamma_{r,0} \rangle, \quad (29)$$

and more generally, the losses of the state $\mathcal{M}$ are given by

$$\langle \Gamma_{r,\mathcal{M}} \rangle = \left(\mathcal{M} + \frac{1}{2} \right) \frac{\pi \Lambda \hbar}{mw^2}. \quad (30)$$

When interactions are present, Eq. (22) becomes

$$\frac{U_0}{\sigma^2} w^4 - \frac{\alpha N}{\sqrt{2\pi}} w - \frac{\hbar^2}{2m} = 0. \quad (31)$$

This is a 4th-order polynomial equation. It is perfectly solvable; however, the expressions of the solutions are quite cumbersome. Among the four solutions only one is real positive, which is the only one we keep since w is a length. To understand the behavior of the system, we consider analytically the two limits $N \to 0$ and $N \to \infty$, which give two different expressions for w by expansion in Laurent series. We find that

$$w_{|N\to 0} \equiv w_-(N) = w_0 - \frac{\alpha\sigma\sqrt{|m|}}{4\hbar\sqrt{2\pi U_0}} N \quad (32)$$

and

$$w_{|N\to\infty} \equiv w_+(N) = \frac{\sqrt{2\pi}\hbar^2}{|m\alpha|N}. \quad (33)$$

The two limits coincide for a value of N that we denote

$$N_{\text{crit}} = \frac{2\hbar}{\alpha} \sqrt{\frac{2\pi\hbar}{|m|\sigma} \sqrt{\frac{U_0}{|m|}}}, \quad (34)$$

obtained by solving the equation $w_- = w_+$. This is the critical value for which interactions within the condensate become the dominant mechanism controlling its width. We can therefore write an approximate expression for the width $w(N)$ using the two asymptotic expressions

$$w \approx w_-\mathcal{U}(-(N - N_{\text{crit}})) + w_+\mathcal{U}(N - N_{\text{crit}}), \quad (35)$$

where $\mathcal{U}$ denotes the Heaviside step function. Figure 2(a) shows the width of the 0 mode versus N, which is here considered as an external parameter. At low N, the mode width is w_0 governed by the reservoir potential. The width then decreases and becomes dominated by the interactions within the condensate for $N > N_{\text{crit}}$. At very large N, the width becomes the same as the one of the bare bright soliton ξ. The full solution of (31) is shown as a thick black line, while the two asymptotic solutions combined by (35) are shown by gold and orange lines.
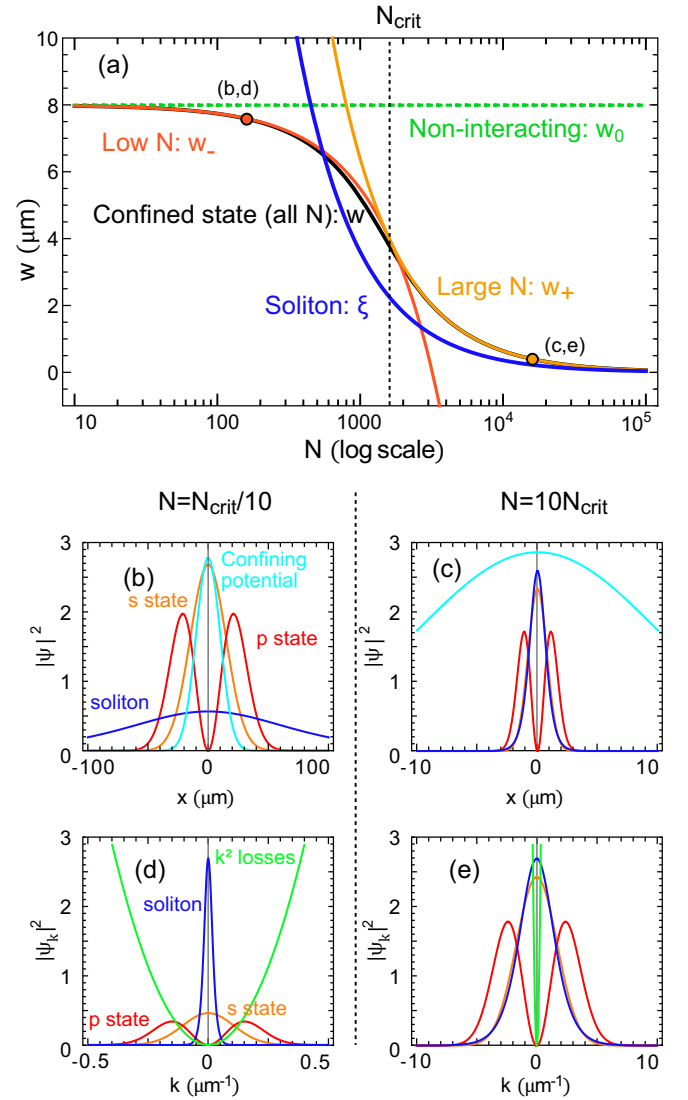

FIG. 2. (a) Width of the Gaussian wave function w (black thick line) and healing length of the soliton ξ (blue line) as a function of the number of particles N. $w_\pm$ (respectively gold/orange lines) are the approximations of w for large/small N, and w_0 is the width in the noninteracting case. (b), (c) Profile of the wave function in real space for $N = N_{\text{crit}}/10$ (b) and $N = 10N_{\text{crit}}$ (c). The confining potential (light blue) has a predominant effect at small N but a small effect at large N. (d), (e) Profile of the wave function in reciprocal space for $N = N_{\text{crit}}/10$ (d) and $N = 10N_{\text{crit}}$ (e). The k^2 losses close to the BIC (green line) give very low losses at low N but high losses at large N. In (b)–(d), the dark blue curve is the soliton wave function and the orange/red curves are the wave functions of the states 0 and 1, respectively.

We now consider the second confined state ψ_1, for which we perform the same type of analysis. We use the spectroscopic notation for the states, as is often done since the polaritonic trap can be considered an artificial atom. The states 0 and 1 therefore correspond to s and p, respectively. We recall that state 1 can host the condensate when the energy of state 0 overcomes the band gap between the BIC and lossy
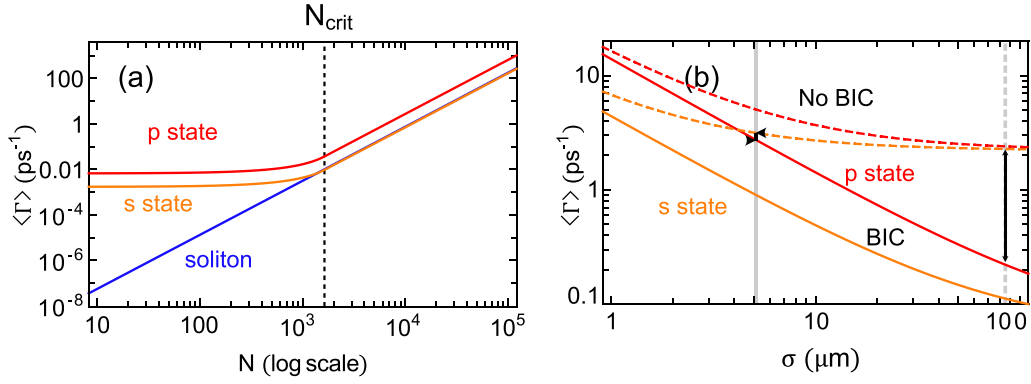
FIG. 3. (a) Losses of the soliton (blue line) and s and p states with respect to the number of particles N (in log-log scale). (b) Losses of the s state (orange lines) and p state (red lines) for a band with a BIC (solid lines) and without a BIC (dashed lines). The left (right) gray line corresponds to the situations of Ref. [41] (Ref. [21]), and the black arrows represent the difference between losses of the s state for a non-BIC state and the p state for a BIC state.

branches. We plot in Figs. 2(b)–2(e) the real- and k-space profiles of the different modes for low N [panels (b), (d)] and large N [panels (c), (e)]. For a low number of particles, the confined states are mostly determined by the width of the confining potential, whereas a free soliton is much broader in real space. On the contrary, for large N, the interactions make all modes narrower so that the confining potential [which does not change between (b) and (c)] has only a minor influence on the width of the confined states, which is close to that of the free soliton.

In k space, the trend is inverse: the narrow states in real space are broad in k space. The broadening in k space for all states increases linearly with the growth of N [Eqs. (16), (33)]. Another important aspect is that the p state shows a node at $k = 0$ and shows, in all cases, a smaller overlap with the BIC resonance compared with the soliton and the s states. On the other hand, for large N, all states are broad in reciprocal space. This means that most of their probability density is located outside the BIC point and, therefore, these states almost do not benefit from the extremely long BIC lifetime.

These features are summarized in Fig. 3(a), which shows the radiative losses of the soliton, the s, and the p states versus N. We observe the N^2 dependence of Γ for the soliton case. We observe at $N = N_{\mathrm{crit}}$ the transition for s and p states from a regime where Γ is fixed by the pump size to a soliton-like regime dominated by the interactions within the condensate. We observe the constant ratio [equal to 3; see Eq. (29)] for the decay rates between the s and p states. The transition occurs at $N = N_{\mathrm{crit}}$. All decay rates Γ depend on the size of the confining potential σ. This is shown in Fig. 3(b), which also includes a comparison with the band that does not contain a BIC (lossy branch) but instead is characterized by a nonradiative decay rate $\langle\Gamma_{\mathrm{other}}\rangle$ (for instance, due to the excitonic resonance when considering exciton-polaritons) and a radiative decay rate $\langle\Gamma_r\rangle$ which does not depend on k (for instance, the losses of a usual mode above the light cone), so that

$$\langle\Gamma\rangle = \langle\Gamma_r\rangle + \langle\Gamma_{\mathrm{other}}\rangle. \tag{36}$$

We observe that for a small reservoir size, the condensate is considerably wider in k space with respect to the range where BIC modifies the decay rate. This situation corresponds approximately to the observation of Ref. [41], where the pump

size is approximately $\sigma \approx 5\,\mu\mathrm{m}$. On the contrary, when the pump size increases, the condensate wave function expands in real space and localizes in k space, overlapping better and better with the BIC resonance. In that case, a band with a BIC shows a much smaller decay rate. This is the regime that was demonstrated in Ref. [21], where the pumping spot has a width $\sigma \approx 80\,\mu\mathrm{m}$. To summarize, using a small pumping spot prevents benefiting from the high lifetime of a BIC.

IV. INFLUENCE OF THE INTERACTIONS ON THE CONDENSATION THRESHOLD

In the previous section, we found analytical formulas for the losses of the soliton and s and p states. We show that the losses depend on the number of particles N. In this section, we use the previously found density-dependent losses to solve the semiclassical Boltzmann equations [58], which describe the evolution of the population of the condensate and reservoir states with time. In the previous sections, the system was assumed to be 1D and uniform in the transverse direction. Here, we need to take into account a normalization surface in order to operate with the populations and scattering rates. Experimentally, operating with a finite-size pump simply leads to additional nonradiative losses due to the repulsion of the particles from the excitation spot due to the interactions. The simplified 2-state model used in this section does not allow us to take into account the details of the relaxation processes that depend on the dispersion relation. Its goal is to focus on the effects of the density-dependent lifetime in the condensate, which is due to the soliton formation. The two coupled equations read

$$\dot{N}_c = W_{\mathrm{LO}}N_x(1 + N_c) - N_c\Gamma_c(N_c), \tag{37}$$

$$\dot{N}_x = -W_{\mathrm{LO}}N_x(1 + N_c) - N_x\Gamma_x + P, \tag{38}$$

where $N_{c,x}$ are, respectively, the numbers of particles in the condensate/reservoir, $\Gamma_{c,x}$ are the condensate/reservoir losses, and P denotes the pumping strength. W_{LO} describes the relaxation of excitons through LO phonons, which we assume to be the dominant relaxation mechanism. Indeed, the design of the structure was optimized in order to have a resonant enhancement for the LO-phonon assisted relaxation:
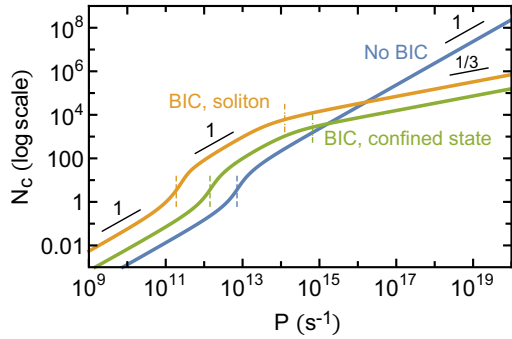
FIG. 4. Number of particles in the condensate N_c versus pumping strength P. The blue line corresponds to the situation without a BIC, the gold line to the situation with a BIC and a free soliton (no confinement), and the green line to the situation with a BIC and confined states (the p state in this case). Short vertical dashed lines indicate the condensation threshold in each situation. Short vertical dash-dotted lines indicate the slope breaks (1 to 1/3) due to the presence of the BIC.

$E_0^{\mathrm{BIC}} = E_X + \frac{3}{2}k_BT - E_{LO}$ at $T = 300\,\mathrm{K}$. W_{LO} is estimated from Ref. [58] to $W_{LO} = 6 \times 10^9\,\mathrm{s}^{-1}$ for the surface we consider. We neglect the dependence of the scattering rate on the spatial shape of the condensate. We solve the Boltzmann equations over time until a stationary configuration is obtained. These simulations are repeated for different values of pumping P. This allows us to obtain the stationary population of the condensate for each pumping.

We consider three different cases, which we plot in Fig. 4. In the first case, we consider a configuration where the condensate is not a BIC. The losses for this state (both radiative and nonradiative) are assumed to be k-independent $\Gamma_c = \langle\Gamma_{\mathrm{nr}}\rangle + \langle\Gamma_{r,0}\rangle$. When increasing the pumping strength, we see that the blue curve exhibits a threshold around $P \approx 10^{13}\,\mathrm{s}^{-1}$, but the slopes before and after the threshold are the same, $N_c \sim P$. For large N_c, the stationary solution can be found analytically as

$$N_c \approx \frac{\hbar P}{\Gamma_c} - \frac{\Gamma_x}{W_{LO}}. \qquad (39)$$

The two other curves show the solutions when the system hosts a BIC. The golden curve represents the solution without confining potential, where the condensate wave function is the one of a soliton. We see that using a BIC instead of an ordinary lossy state reduces the threshold required for condensation by approximately two orders of magnitude (the threshold is estimated to be reached for $N_c \approx 3$). Before and just after the threshold, the condensate population evolves linearly versus P, as in the case without the BIC. However, far above threshold, when $N_c \approx 10^4$, the dependence changes due to the formation of the soliton, whose losses scale as N_c^2, as shown in Eq. (17). In that regime, keeping only leading terms in N_c one can find the asymptotic dependence of N_c versus P as

$$N_c \approx \left(\frac{\hbar P}{\beta}\right)^{1/3}, \qquad (40)$$

which corresponds to the 1/3 slope we observe in the numerical results at large N_c.

Finally, the green curve is obtained when considering a BIC with both confinement by an exciton reservoir and self-interactions. In this case, the losses are given by Eq. (29), and the width is taken from the solution of Eq. (31) (the analytical exact solution, not the approximate solutions). We take the losses of state 1 (the p state) in order to reproduce the situation studied experimentally in Ref. [41]. The solution for state 0 (s state) is not plotted because it is very similar to the one we found considering only the soliton without confinement. Indeed, for large N_c, the losses of state 0 are close to the soliton losses, and for small N_c, the solutions of Boltzmann equations are less influenced by N-dependent losses. We see that the green curve is an intermediate case between the soliton located at a BIC and a usual configuration with a BIC: the threshold is higher than with the BIC and without confinement, but the interactions limit the growth of N_c at large values with the same power law. Modifying the width of the confinement potential allows changing the threshold value: the narrower the potential, the higher the threshold.

To conclude, in this section we have shown that the BIC can be beneficial to reduce the threshold. However, the interactions deeply modify the behavior at large pumping strengths/number of particles because the dependence between the two parameters becomes sublinear. Finally, the size of the reservoir can reduce the effects of the BIC.

V. NUMERICAL SIMULATIONS OF POLARITON CONDENSATION WITH GROSS-PITAEVSKII EQUATION

In this section, we solve numerically the Gross-Pitaevskii equation to verify qualitatively the validity of the hypotheses used and results obtained in the previous sections. The studies performed in the previous sections were based on the hypothesis that the shape of the condensate wave function is a solution to the conservative GP equation. The role of the pumping and lifetime is to set the number of particles in the condensate, which is a wave function parameter. We did not consider that the k-dependent lifetime itself could deeply affect the shape of the condensate wave function. In order to take into account on an equal footing interaction and lifetime effects, we solve numerically the hybrid Boltzmann–Gross-Pitaevskii equation, including the scattering from a localized excitonic reservoir and k-dependent lifetime, similar to what is usually done to describe energy relaxation [43,59]. The goal here is to check the validity of the analytical predictions for the shape of the condensate and simulate the emission pattern observed in experiments, and not to obtain a quantitative estimate of the threshold, which is why we eliminate the equation for the reservoir. The equation reads

$$i\hbar\frac{\partial}{\partial t}\psi(x,t) = \left((i\Lambda - 1)\frac{\hbar^2}{2m}\frac{\partial^2}{\partial x^2} + \alpha(|\psi(x,t)|^2 + 2n_x(x))\right.$$
$$\left. + i\hbar[W_{LO}n_x(x)e^{-N_x/N_{\mathrm{sat}}} - \Gamma_0]\right)\psi(x,t)$$
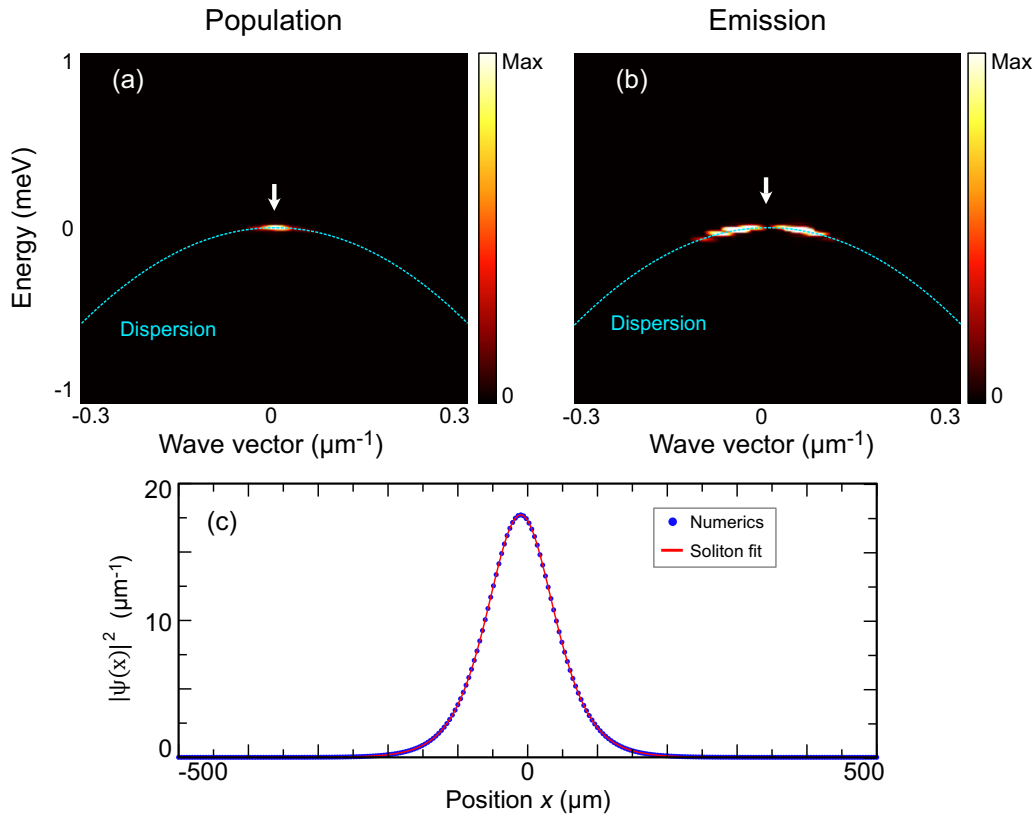$$+ \chi(x,t), \qquad (41)$$

FIG. 5. Polariton Bose-Einstein condensate in a BIC. (a), (b) Numerical results of the simulation of the Gross-Pitaevskii equation (41) for the BIC LPB (containing a BIC at $k = 0$). (a) Population in the reciprocal space. Note the unique intensity peak at the maximum of the dispersion (at the BIC). (b) Numerically calculated emission in the reciprocal space. Note the two peaks surrounding $k = 0$. In both panels, the dispersion is indicated as a cyan dashed line, and a white arrow shows the position of the BIC (state) in reciprocal space. (c) Numerically obtained distribution of particles in real space (blue points) after the stationary regime is reached and fitted by a bright soliton wave function (red line). Note the excellent agreement.

where $m = -(1.5 \pm 0.1)10^{-6}m_0$, $\Lambda = -(0.27 \pm 0.03)$ as obtained in the first section. $n_x(x)$ is the reservoir density, which we assume to keep the spatial profile of the pumping laser and to be constant in time. The reservoir depletion is taken into account via the saturated gain term. We add a noise term $\chi(x, t)$ to simulate the spontaneous scattering into the polaritonic modes from the reservoir. The filling of the condensate from an excitonic reservoir generated by a nonresonant optical pumping is assumed to be assisted by the LO phonons through the term containing the LO phonon scattering matrix element W_{LO}. The saturation is controlled by the total number of particles in the reservoir $N_x = \int n(x)dx$ and its saturation value N_{sat}, which in the Boltzmann equations is controlled by the pumping P via the second equation (38) that we eliminate adiabatically here. The interaction constant α describes polariton-polariton interaction. A twice larger value for the reservoir excitons is taken in the hypothesis of zero detuning operation. Here, the normalization area for both α and W_{LO} is taken equal to the spatial grid size 2 μm times the transverse pump size 20 μm. The main difference between our design and the one presented in Ref. [60] is that our BIC is a polaritonic BIC and not just a photonic BIC, which enlarges the potential applications of our proposal compared to this previous realization. The goal of these simulations is

to demonstrate that the interactions lead to the formation of a soliton, that its reciprocal-space image corresponds to the one observed experimentally, and that its shape is very close to the one considered analytically.

We show the results of numerical simulations based on Eq. (41) in Fig. 5 using a homogeneous reservoir profile. The time-dependent simulation is run until a stationary solution is achieved. Above threshold (which in our simulations occurs well below the Mott density), a condensate forms in the ground state of the system, but the interactions lead to its localization in real space and spreading in reciprocal space, as expected. Panel (a) shows the condensate distribution in reciprocal space $|\psi(k)|^2$. We can see that the population is maximal at the top of the dispersion (the dispersion is indicated by a cyan dashed line), which is precisely the position of the BIC. Indeed, the BIC has fewer losses than any other mode, so the condensation occurs there.

In most of the systems exhibiting polariton condensation, a higher population corresponds to a higher intensity of emitted light (but even for usual polaritons, one has to take into account the photonic fraction to determine the polariton population from the emission intensity [61]). In the case of BICs, the population is very different from the emission. Indeed, the light emitted by the structure is proportional to the losses: the

light that is collected is the light that escaped the waveguide and impinges onto the detector. The emission $\Gamma_r(k)|\psi(k)|^2$ is plotted in panel (b). We can see two peaks close to the maximum of the dispersion, corresponding to the experimental observation of the polariton condensation at the BICs [21]. The population is huge in the BIC, but the emission is very low precisely because the lifetime is very high, larger than for the modes close in reciprocal space, which still have a very high population. In the end, we only see two peaks of emission close to the BIC, but not the BIC itself.

Our numerical simulations using the Gross-Pitaevskii equation confirm the formation of bright solitons due to the interactions. We plot in Fig. 5(c) the distribution of particles in real space calculated numerically after condensation and after the system has stabilized (the condensation occurs after 20 ps and the picture is taken after 15 ns). We see that there is one peak (blue numerical points) that is well fitted by the wave function of a bright soliton (red line), as given by Eq. (13). The shape corresponds very well to the profile found in the conservative approximation in the previous sections, which confirms the validity of our analytical considerations. Note that the formation of solitons and their interplay with BICs in a different (resonant) pumping configuration have been theoretically discussed in Refs. [62,63]. However, we observe numerically an additional effect. When the number of particles exceeds a critical value, the system becomes unstable and does not converge to a stationary solution. This may lead to the formation of several solitons that exhibit periodic oscillations, without merging into a single soliton. According to our analysis, this is not due to the Kibble-Zurek mechanism [64,65], which has already been proposed to explain different effects in polaritonic structures [66–68]. The effect is rather due to an analog of modulational instability, but in a driven-dissipative system. A detailed study of this phenomenon exceeds the scope of the present article and requires further investigations.

VI. CONCLUSIONS

To conclude, we design a structure for polariton Bose-Einstein condensation (polariton lasing) based on a 1D BIC in a TiO_2-GaN waveguide. We predict a possible realization of room-temperature polariton Bose-Einstein condensation in the BIC state. This could be implemented using state-of-the-art experimental techniques. It would allow obtaining an electrically injected room-temperature polariton laser with a low lasing threshold. We also investigate how to benefit from the high lifetime of the BIC in photonic structures with interacting particles (for instance, structures based on wide-band-gap semiconductors and TMDs, where interactions between polaritons are strong). It requires working with the largest structure possible to access the smallest wave vector and the highest lifetimes, and the pumping spot needs to be sufficiently large as well, to prevent confinement effects from reducing the lifetime of the BIC. Soliton formation due to the interactions can increase the losses above threshold. An interesting perspective is to consider the condensation of interacting particles in 2D BICs.

[1] E. Noether, Nachrichten der Königlichen Gesellschaft der Wissenschaften zu Göttingen, Math.-phys. Klasse **2**, 235 (1918).

[2] G. Lindblad, On the generators of quantum dynamical semigroups, Commun. Math. Phys. **48**, 119 (1976).

[3] M. Król, I. Septembre, P. Oliwa, M. Kędziora, K. Łempicka-Mirek, M. Muszyński, R. Mazur, P. Morawiak, W. Piecek, P. Kula *et al.*, Annihilation of exceptional points from different Dirac valleys in a 2D photonic system, Nat. Commun. **13**, 5340 (2022).

[4] C. M. Bender and S. Boettcher, Real spectra in non-Hermitian Hamiltonians having $\mathcal{PT}$ symmetry, Phys. Rev. Lett. **80**, 5243 (1998).

[5] E. J. Bergholtz, J. C. Budich, and F. K. Kunst, Exceptional topology of non-Hermitian systems, Rev. Mod. Phys. **93**, 015005 (2021).

[6] B. Peng, Ş. K. Özdemir, M. Liertzer, W. Chen, J. Kramer, H. Yılmaz, J. Wiersig, S. Rotter, and L. Yang, Chiral modes and directional lasing at exceptional points, Proc. Natl. Acad. Sci. USA **113**, 6845 (2016).

[7] S. Yao and Z. Wang, Edge states and topological invariants of non-Hermitian systems, Phys. Rev. Lett. **121**, 086803 (2018).

[8] P. Kokhanchik, D. D. Solnyshkov, and G. Malpuech, Non-Hermitian skin effect induced by Rashba-Dresselhaus spin-orbit coupling, Phys. Rev. B **108**, L041403 (2023).

[9] H. Friedrich and D. Wintgen, Interfering resonances and bound states in the continuum, Phys. Rev. A **32**, 3231 (1985).

[10] A. Z. Devdariani, V. N. Ostrovskii, and Y. N. Sebyakin, Crossing of quasistationary levels, ZhETF **71**, 909 (1976) [Sov. Phys. JETP **44**, 477 (1976)].

[11] C. W. Hsu, B. Zhen, A. D. Stone, J. D. Joannopoulos, and M. Soljačić, Bound states in the continuum, Nat. Rev. Mater. **1**, 16048 (2016).

[12] J. von Neuman and E. Wigner, Uber merkwürdige diskrete Eigenwerte. Uber das Verhalten von Eigenwerten bei adiabatischen Prozessen, Phys. Z. **30**, 467 (1929).

[13] S. I. Azzam and A. V. Kildishev, Photonic bound states in the continuum: From basics to applications, Adv. Opt. Mater. **9**, 2001469 (2021).

[14] H. Matsubara, S. Yoshimoto, H. Saito, Y. Jianglin, Y. Tanaka, and S. Noda, GaN photonic-crystal surface-emitting laser at blue-violet wavelengths, Science **319**, 445 (2008).

[15] D. D. Solnyshkov, T. Weiss, G. Malpuech, and N. A. Gippius, Polariton laser based on a ZnO photonic crystal slab, Appl. Phys. Lett. **99**, 111110 (2011).

[16] V. Kravtsov, E. Khestanova, F. A. Benimetskiy, T. Ivanova, A. K. Samusev, I. S. Sinev, D. Pidgayko, A. M. Mozharov, I. S. Mukhin, M. S. Lozhkin *et al.*, Nonlinear polaritons in a monolayer semiconductor coupled to optical bound states in the continuum, Light Sci. Appl. **9**, 56 (2020).

[17] N. Bernhardt, K. Koshelev, S. J. White, K. W. C. Meng, J. E. Froch, S. Kim, T. T. Tran, D.-Y. Choi, Y. Kivshar, and A. S. Solntsev, Quasi-BIC resonant enhancement of second-harmonic generation in WS_2 monolayers, Nano Lett. **20**, 5309 (2020).

[18] E. Maggiolini, L. Polimeno, F. Todisco, A. Di Renzo, B. Han, M. De Giorgi, V. Ardizzone, C. Schneider, R. Mastria, A. Cannavale *et al.*, Strongly enhanced light-matter coupling of monolayer WS_2 from a bound state in the continuum, Nat. Mater. **22**, 964 (2023).

[19] A. Grudinina, M. Efthymiou-Tsironi, V. Ardizzone, F. Riminucci, M. D. Giorgi, D. Trypogeorgos, K. Baldwin, L. Pfeiffer, D. Ballarini, D. Sanvitto *et al.*, Collective excitations of a bound-in-the-continuum condensate, Nat. Commun. **14**, 3464 (2023).

[20] A. Gianfrate, H. Sigurðsson, V. Ardizzone, H. C. Nguyen, F. Riminucci, M. Efthymiou-Tsironi, K. W. Baldwin, L. N. Pfeiffer, D. Trypogeorgos, M. De Giorgi *et al.*, Reconfigurable quantum fluid molecules of bound states in the continuum, Nat. Phys. **20**, 61 (2024).

[21] V. Ardizzone, F. Riminucci, S. Zanotti, A. Gianfrate, M. Efthymiou-Tsironi, D. Suàrez-Forero, F. Todisco, M. De Giorgi, D. Trypogeorgos, G. Gigli *et al.*, Polariton Bose-Einstein condensate from a bound state in the continuum, Nature (London) **605**, 447 (2022).

[22] F. Riminucci, V. Ardizzone, L. Francaviglia, M. Lorenzon, C. Stavrakas, S. Dhuey, A. Schwartzberg, S. Zanotti, D. Gerace, K. Baldwin *et al.*, Nanostructured GaAs/(Al,Ga)As waveguide for low-density polariton condensation from a bound state in the continuum, Phys. Rev. Appl. **18**, 024039 (2022).

[23] A. Imamoglu, R. J. Ram, S. Pau, and Y. Yamamoto, Nonequilibrium condensates and lasers without inversion: Exciton-polariton lasers, Phys. Rev. A **53**, 4250 (1996).

[24] A. Kavokin, J. J. Baumberg, G. Malpuech, and F. P. Laussy, *Microcavities* (Oxford University Press, 2017).

[25] L. Pitaevskii and S. Stringari, *Bose-Einstein Condensation* (Oxford Science Publications, 2003).

[26] D. Tanese, H. Flayac, D. D. Solnyshkov, A. Amo, A. Lemaître, E. Galopin, R. Braive, P. Senellart, I. Sagnes, G. Malpuech *et al.*, Polariton condensation in solitonic gap states in a one-dimensional periodic potential, Nat. Commun. **4**, 1749 (2013).

[27] N. Pernet, P. St-Jean, D. D. Solnyshkov, G. Malpuech, N. Carlon Zambon, Q. Fontaine, B. Real, O. Jamadi, A. Lemaitre, M. Morassi *et al.*, Gap solitons in a one-dimensional driven-dissipative topological lattice, Nat. Phys. **18**, 678 (2022).

[28] M. Milićević, O. Bleu, D. D. Solnyshkov, I. Sagnes, A. Lemaître, L. Le Gratiet, A. Harouri, J. Bloch, G. Malpuech, and A. Amo, Lasing in optically induced gap states in photonic graphene, SciPost Phys. **5**, 064 (2018).

[29] T. Jacqmin, I. Carusotto, I. Sagnes, M. Abbarchi, D. D. Solnyshkov, G. Malpuech, E. Galopin, A. Lemaître, J. Bloch, and A. Amo, Direct observation of Dirac cones and a flatband in a honeycomb lattice for polaritons, Phys. Rev. Lett. **112**, 116402 (2014).

[30] M. Zamfirescu, A. Kavokin, B. Gil, G. Malpuech, and M. Kaliteevski, ZnO as a material mostly adapted for the realization of room-temperature polariton lasers, Phys. Rev. B **65**, 161205(R) (2002).

[31] F. Li, L. Orosz, O. Kamoun, S. Bouchoule, C. Brimont, P. Disseix, T. Guillet, X. Lafosse, M. Leroux, J. Leymarie, M. Mexis, M. Mihailovic, G. Patriarche, F. Réveret, D. Solnyshkov, J. Zúñiga-Pérez, and G. Malpuech, From excitonic to photonic polariton condensate in a ZnO-based microcavity, Phys. Rev. Lett. **110**, 196406 (2013).

[32] O. Jamadi, F. Reveret, P. Disseix, F. Medard, J. Leymarie, A. Moreau, D. Solnyshkov, C. Deparis, M. Leroux, E. Cambril *et al.*, Edge-emitting polariton laser and amplifier based on a ZnO waveguide, Light Sci. Appl. **7**, 82 (2018).

[33] G. Malpuech, A. Di Carlo, A. Kavokin, J. Baumberg, M. Zamfirescu, and P. Lugli, Room-temperature polariton lasers based on GaN microcavities, Appl. Phys. Lett. **81**, 412 (2002).

[34] S. Christopoulos, G. B. H. von Högersthal, A. J. D. Grundy, P. G. Lagoudakis, A. V. Kavokin, J. J. Baumberg, G. Christmann, R. Butté, E. Feltin, J.-F. Carlin, and N. Grandjean, Room-temperature polariton lasing in semiconductor microcavities, Phys. Rev. Lett. **98**, 126405 (2007).

[35] H. Souissi, M. Gromovyi, T. Gueye, C. Brimont, L. Doyennette, D. D. Solnyshkov, G. Malpuech, E. Cambril, S. Bouchoule, B. Alloing, S. Rennesson, F. Semond, J. Zúñiga-Pérez, and T. Guillet, Ridge polariton laser: Different from a semiconductor edge-emitting laser, Phys. Rev. Appl. **18**, 044029 (2022).

[36] S. Kéna-Cohen and S. Forrest, Room-temperature polariton lasing in an organic single-crystal microcavity, Nat. Photonics **4**, 371 (2010).

[37] J. D. Plumhof, T. Stöferle, L. Mai, U. Scherf, and R. F. Mahrt, Room-temperature Bose-Einstein condensation of cavity exciton-polaritons in a polymer, Nat. Mater. **13**, 247 (2014).

[38] R. Su, C. Diederichs, J. Wang, T. C. Liew, J. Zhao, S. Liu, W. Xu, Z. Chen, and Q. Xiong, Room-temperature polariton lasing in all-inorganic perovskite nanoplatelets, Nano Lett. **17**, 3982 (2017).

[39] R. Su, S. Ghosh, J. Wang, S. Liu, C. Diederichs, T. C. Liew, and Q. Xiong, Observation of exciton polariton condensation in a perovskite lattice at room temperature, Nat. Phys. **16**, 301 (2020).

[40] K. Peng, R. Tao, L. Haeberlé, Q. Li, D. Jin, G. R. Fleming, S. Kéna-Cohen, X. Zhang, and W. Bao, Room-temperature polariton quantum fluids in halide perovskites, Nat. Commun. **13**, 7388 (2022).

[41] F. Riminucci, A. Gianfrate, D. Nigro, V. Ardizzone, S. Dhuey, L. Francaviglia, K. Baldwin, L. N. Pfeiffer, D. Ballarini, D. Trypogeorgos, A. Schwartzberg *et al.*, Polariton condensation in gap-confined states of photonic crystal waveguides, Phys. Rev. Lett. **131**, 246901 (2023).

[42] D. Nigro and D. Gerace, Theory of exciton-polariton condensation in gap-confined eigenmodes, Phys. Rev. B **108**, 085305 (2023).

[43] D. D. Solnyshkov, H. Terças, K. Dini, and G. Malpuech, Hybrid Boltzmann–Gross-Pitaevskii theory of Bose-Einstein condensation and superfluidity in open driven-dissipative systems, Phys. Rev. A **89**, 033626 (2014).

[44] G. Christmann, R. Butté, E. Feltin, A. Mouti, P. A. Stadelmann, A. Castiglia, J.-F. Carlin, and N. Grandjean, Large vacuum Rabi splitting in a multiple quantum well GaN-based microcavity in the strong-coupling regime, Phys. Rev. B **77**, 085310 (2008).

[45] C. Brimont, L. Doyennette, G. Kreyder, F. Réveret, P. Disseix, F. Médard, J. Leymarie, E. Cambril, S. Bouchoule, M. Gromovyi *et al.*, Strong coupling of exciton-polaritons in a bulk GaN planar waveguide: Quantifying the coupling strength, Phys. Rev. Appl. **14**, 054060 (2020).

[46] L. Mallet-Dida, P. Disseix, F. Réveret, F. Médard, B. Alloing, J. Zúñiga-Pérez, and J. Leymarie, The low temperature limit of the excitonic Mott density in GaN: An experimental reassessment, New J. Phys. **24**, 033031 (2022).

[47] I. Septembre, C. Leblanc, L. Hermet, H. S. Nguyen, X. Letartre, D. D. Solnyshkov, and G. Malpuech, Design of a room-temperature topological exciton-polariton laser in a ZnO/TiO$_2$ photonic crystal slab, Phys. Rev. B **107**, 155304 (2023).

[48] H. Souissi, M. Gromovyi, I. Septembre, V. Develay, C. Brimont, L. Doyennette, E. Cambril, S. Bouchoule, B. Alloing, E. Frayssinet, J. Zúñiga-Pérez *et al.*, Mode-locked GaN waveguide polariton laser, arXiv:2310.18661.

[49] O. Jamadi, F. Réveret, E. Mallet, P. Disseix, F. Médard, M. Mihailovic, D. Solnyshkov, G. Malpuech, J. Leymarie, X. Lafosse, S. Bouchoule, F. Li, M. Leroux, F. Semond, and J. Zúñiga-Pérez, Polariton condensation phase diagram in wide-band-gap planar microcavities: GaN versus ZnO, Phys. Rev. B **93**, 115205 (2016).

[50] J. Ciers, D. D. Solnyshkov, G. Callsen, Y. Kuang, J.-F. Carlin, G. Malpuech, R. Butté, and N. Grandjean, Polariton relaxation and polariton nonlinearities in nonresonantly cw-pumped III-nitride slab waveguides, Phys. Rev. B **102**, 155304 (2020).

[51] G. Christmann, D. Simeonov, R. Butté, E. Feltin, J.-F. Carlin, and N. Grandjean, Impact of disorder on high quality factor III-V nitride microcavities, Appl. Phys. Lett. **89**, 261101 (2006).

[52] J. Levrat, R. Butté, E. Feltin, J.-F. Carlin, N. Grandjean, D. Solnyshkov, and G. Malpuech, Condensation phase diagram of cavity polaritons in GaN-based microcavities: Experiment and theory, Phys. Rev. B **81**, 125305 (2010).

[53] S. Dufferwiel, T. P. Lyons, D. D. Solnyshkov, A. A. Trichet, F. Withers, S. Schwarz, G. Malpuech, J. M. Smith, K. S. Novoselov, M. S. Skolnick *et al.*, Valley-addressable polaritons in atomically thin semiconductors, Nat. Photonics **11**, 497 (2017).

[54] J. Gu, V. Walther, L. Waldecker, D. Rhodes, A. Raja, J. C. Hone, T. F. Heinz, S. Kéna-Cohen, T. Pohl, and V. M. Menon, Enhanced nonlinear interaction of polaritons via excitonic Rydberg states in monolayer WSe$_2$, Nat. Commun. **12**, 2269 (2021).

[55] C. Louca, A. Genco, S. Chiavazzo, T. P. Lyons, S. Randerson, C. Trovatello, P. Claronino, R. Jayaprakash, X. Hu, J. Howarth *et al.*, Interspecies exciton interactions lead to enhanced nonlinearity of dipolar excitons and polaritons in MoS$_2$ homobilayers, Nat. Commun. **14**, 3818 (2023).

[56] L. D. Landau and E. M. Lifshitz, *Quantum Mechanics: Non-Relativistic Theory* (Elsevier, 2013), Vol. 3.

[57] D. D. Solnyshkov, I. Septembre, K. Ndiaye, and G. Malpuech, Analog of Foucault precession in two-dimensional quantum harmonic oscillators with Berry curvature, Phys. Rev. B **108**, 144306 (2023).

[58] A. Kavokin and G. Malpuech, *Cavity Polaritons* (Elsevier, 2003).

[59] E. Wertz, A. Amo, D. D. Solnyshkov, L. Ferrier, T. C. H. Liew, D. Sanvitto, P. Senellart, I. Sagnes, A. Lemaître, A. V. Kavokin, G. Malpuech, and J. Bloch, Propagation and amplification dynamics of 1D polariton condensates, Phys. Rev. Lett. **109**, 216404 (2012).

[60] X. Wu, J. Song, S. Zhang, W. Du, Y. Wang, Z. Zhu, Y. Liang, Q. Zhang, Q. Xiong, and X. Liu, Room-temperature bound states in the continuum polariton condensation, arXiv:2303.09923.

[61] J. Kasprzak, M. Richard, S. Kundermann, A. Baas, P. Jeambrun, J. M. J. Keeling, F. Marchetti, M. Szymańska, R. André, J. Staehli *et al.*, Bose-Einstein condensation of exciton polaritons, Nature (London) **443**, 409 (2006).

[62] D. Dolinina and A. Yulin, Dissipative switching waves and solitons in the systems with spontaneously broken symmetry, Phys. Rev. E **103**, 052207 (2021).

[63] D. Dolinina and A. Yulin, Interactions of the solitons in periodic driven-dissipative systems supporting quasibound states in the continuum, Phys. Rev. E **104**, 054214 (2021).

[64] T. W. B. Kibble, Topology of cosmic domains and strings, J. Phys. A: Math. Gen. **9**, 1387 (1976).

[65] W. H. Zurek, Cosmological experiments in superfluid helium? Nature (London) **317**, 505 (1985).

[66] D. D. Solnyshkov, A. V. Nalitov, and G. Malpuech, Kibble-Zurek mechanism in topologically nontrivial zigzag chains of polariton micropillars, Phys. Rev. Lett. **116**, 046402 (2016).

[67] D. D. Solnyshkov, L. Bessonart, A. Nalitov, and G. Malpuech, Kibble-Zurek mechanism in polariton graphene, Phys. Rev. B **104**, 035423 (2021).

[68] D. D. Solnyshkov, C. Leblanc, I. Septembre, and G. Malpuech, Domain-wall topology induced by spontaneous symmetry breaking in polariton graphene, Phys. Rev. Lett. **129**, 066802 (2022).